Ceramic Capacitors: Turning a Deficiency into an Advantage

Shmuel (Sam) Ben-Yaakov, *Life Fellow, IEEE*
Department of Electrical and Computer Engineering
Ben-Gurion University of the Negev
P.O. Box 653, Beer-Sheva, 8410501 Israel
sby@bgu.ac.il
http://www.ee.bgu.ac.il/~pel

Ilya Zeltser
Power Electronics Department
Rafael Advanced Defense Systems Ltd.
P.O. Box 2250, Haifa 3102102, Israel
ilyaz@rafael.co.il
www.rafael.co.il

***Abstract* - The feasibility of applying standard commercial ceramic capacitors (CC) for controlling a series resonant converter was examined by a simulation model that was calibrated experimentally. The study reveals that the CC could be a viable control element for resonant converters. It is shown that CC controlled series resonant converter can be operated under ZVS. The results of this study show that control attributes of the capacitor controlled SRC are identical to those of the conventional frequency controlled SRC, if the range of the capacitor change is equal to the range of the frequency change in the conventional converter, squared. Based on the present investigation, capacitance ratios of 1:5 can be practically achieved with commercial CC. It was found that the nonlinearity nature of the CC has only a minor effect due to the narrow bandwidth nature of resonant converters.**

Keywords - Ceramic capacitors; ferroelectric dielectric; simulation; SPICE; voltage dependent capacitors; series resonant converter; soft switching; capacitor's driver

I. Introduction

Ceramic capacitors (CC) are being used extensively in power electronics circuits as they have a multitude of advantages that match power conversion circuits' requirements. Having a high dielectric constant, the CC are of small size and by proper design they can withstand high voltages. Furthermore, they have a relatively low equivalent series resistance (ESR) and are compatible with high switching frequencies to about 10MHz. And finally, the CC are relatively inexpensive and thus compatible with current cost-effective design trends. Some CC dielectric materials, notably the COG, are temperature stable and some CC dielectric materials are relatively insensitive to bias voltage. But small size CC with high dielectric constant material, like X5V, are extremely sensitive to bias voltage. For example, the X5V based CC drop to 20% of their initial value when exposed to the maximum allowable voltage. The bias dependence problem is usually "solved" by specifying larger capacitances such that the required capacitance will be assured at the operating point.

This preliminary investigation examines the possibility of turning the voltage dependence deficiency of CC into an advantage. In particular, using the CC as a control element, notably in resonant circuits. The idea of using variable reactive elements for tuning resonant circuits has been explored in the past. For example, the use of a variable inductor to control resonant converters was shown in [1-3] and the possibility of applying CC to control converters was studied in some earlier papers [4-8].

A switched-capacitor was used to emulate a variable capacitor and then applied for auto tuning of a resonant circuit [9], while a switched capacitor bank was applied to control a resonant LLC converter [10]. Commercial dielectric materials and CC have been extensively studied, characterized and modeled in the past [e.g. 11-28].

The primary objective of this study is to characterize the voltage dependent CC features when applied to control resonant circuits. The study has been carried out on the series resonant converter to explore the generic behavior of capacitor controlled resonant circuits. This work discusses only the case of Series Resonant Converter (SRC).

II. Capacitor controlled SRC

The conventional control method of a classical SRC (Fig. 1a) is by a variable frequency. The input to output voltage ratio is normally derived by analyzing the small signal equivalent circuit (Fig. 1b), applying the first harmonics approximation of [29] for the AC load resistance $R_{ac} = \frac{8}{\pi^2}\frac{n_1^2}{n_2^2}R_{load}$, where the parameters are per Fig. 1a and v_{in} is the sinusoidal input drive, which magnitude is related to the DC input voltage of the half bridge SRC, V_{in}, by $v_{in} = \frac{2}{\pi}V_{in}$; v_{out} is the voltage across R_{ac} related to the DC load R_{load} output voltage, V_{out}, by, $v_{out} = \frac{4}{\pi}V_{out}$. Based on Fig. 1b the voltage ratio transfer function is

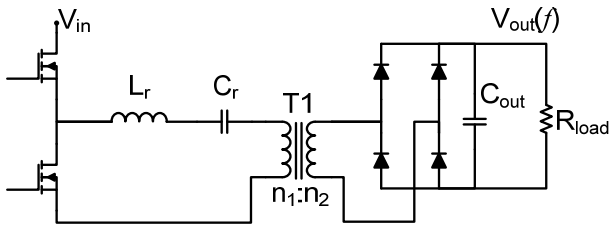

(a)

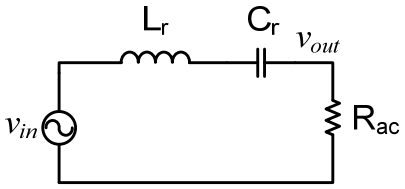

(b)

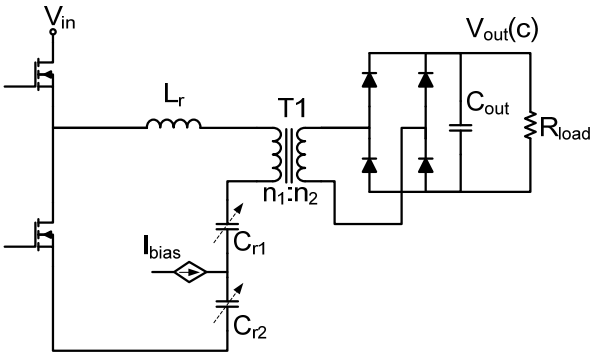

(c)

Fig. 1. SRC. (a) Classical half bridge SRC, (b) Small signal R_{ac} model of a SRC converter, (c) Variable capacitor controlled half bridge SRC.

$$\frac{v_{out}}{v_{in}}(f)=\frac{1}{\sqrt{1+Q^2\left(\frac{f}{f_0}-\frac{f_0}{f}\right)^2}} \qquad (1)$$

where f is the sinusoidal drive frequency, f_0 is the resonant frequency, $f_0 = 1/2\pi\sqrt{L_r C_r}$, and $Q=\sqrt{L_r/C_r}/R_{ac}$.

Typical small signal gain curves of the classical SRC with Q as a parameter are shown in Fig 2a.

The small signal voltage gain of a capacitor controlled SRC (Fig. 1c) is depicted in Fig. 2b. The curves of this plot were obtained by defining a base capacitor C_s for a fixed switching frequency f_s and using it to convert the frequency ratio into a capacitance ratio. This leads to the normalized small signal input to output voltage transfer ratio of the capacitor controlled SRC, in which the switching frequency f_s is fixed.

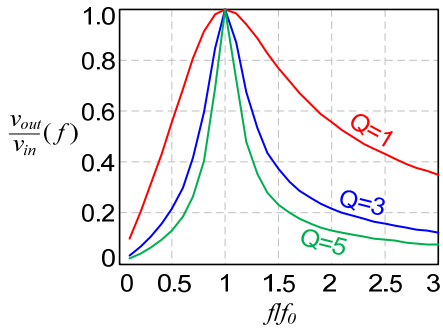

(a)

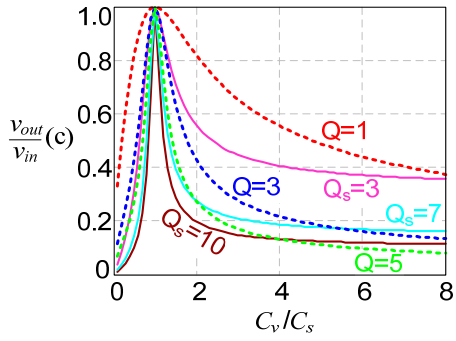

(b)

Fig. 2. Voltage gain magnitude. (a) Classical frequency controlled SRC (b) Variable capacitor controlled SRC.

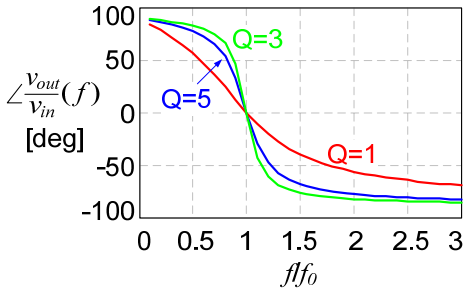

(a)

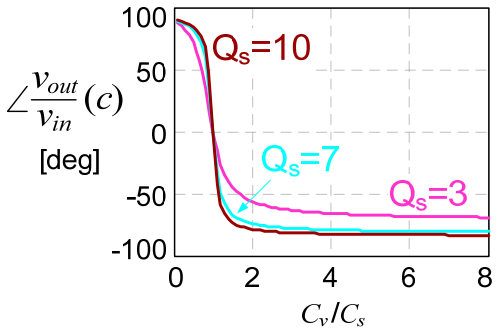

(b)

Fig. 3. Phase of the voltage transfer ratio. (a) Classical frequency controlled SRC (b) Variable capacitor controlled SRC.

$$\frac{v_{out}}{v_{in}}(c)=\frac{1}{\sqrt{1+Q_s^2\left(1-\frac{C_s}{C_v}\right)^2}} \quad (2)$$

where $C_s=\frac{1}{4\pi^2 L_r f_s^2}$; $\frac{f_s}{f_0}=\frac{2\pi\sqrt{L_r C_v}}{2\pi\sqrt{L_r C_s}}=\sqrt{\frac{C_v}{C_s}}$; $Q_s=\frac{\sqrt{L_r/C_s}}{R_{ac}}$

It should be noted that for the same resonant tank inductance, L_r, and load resistance, R_{ac}, the ratio of Q_s to Q is:

$$\frac{Q_s}{Q}=\sqrt{\frac{C_v}{C_s}} \quad (3)$$

To help compare the response of the capacitor controlled SRC to the conventional frequency controlled one, both Q and Q_s are plotted in Fig. 2b. It should also be noted that, according to (2), f_s/f_o is equal to the square root of C_v/C_s, so the scales of Fig. 2a and 2b axis were plotted differently.

The phase plots (Fig. 3a, 3b) show that in the two converters, the phase of the source currents is lagging with respect to the input voltage at frequencies which are higher than the resonant frequency of the relevant Q plot. This implies that operation at this region facilitates zero voltage switching (ZVS) both in the classical and in the capacitor controlled SRC.

The equivalent capacitor C_v in (2) represents the capacitance of the serially connected C_{r1} and C_{r2} (Fig. 1c). C_{r1} is required to block the DC path from the bias source to the half bridge. C_{r1} could be a fixed voltage-insensitive capacitor, with the capacitance much larger than that of the resonant capacitor C_{r2}, or a voltage dependent capacitor, similar to C_{r2}. In the fixed C_{r1} solution, a lower overall ESR of the two capacitors may be achieved, but the physical dimensions of C_{r1} will be larger. In the latter case, the capacitors assembly will be more compact. In this case, the range of change of the capacitance will be affected by the input voltage to the resonant network.

Considering a symmetrical drive of the half bridge (Fig. 2c) and a bias voltage V_{bias} at the midpoint between the two capacitors, the voltage across the upper capacitor, C_{r2}, will be $(V_{bias}-V_{in}/2)$

The DC bias source needs to have a high output impedance, so not to load the resonant network. The proposed driver, whose block diagram is shown in Fig. 4, fulfills this requirement by having the collectors of BJTs at its output. These output BJTs are driven by level shifters that have dead zone at their inputs, set by the comparators B_1, B_2, to prevent a shoot through current through the BJTs. Optimization of the control and the selection of the optimal commercial CCs are beyond the scope of this paper.

The normalized voltage gain ratio of the capacitor controlled SRC is shown in Fig. 2b for three Q_s values. Similar to the case of the classical frequency controlled SRC, the ZVS range for the CC controlled SRC is to the right of the peaks, which are at $C_v/C_s=1$. This is due to the fact that when $C_v/C_s>1$ the resonant frequency of the SRC is below the operating frequency f_s.

Further examination of Fig. 2a reveals that the response of the capacitor controlled SRC is in fact identical to that of the frequency controlled one when taking into account that $\frac{f_s}{f_0}=\sqrt{\frac{C_v}{C_s}}$. For example, the gain of Q=3 curve in Fig. 2a for the frequency ratio $f_s/f_o=2$ is approximately 0.2 and so is the gain for same Q in the capacitor controlled SRC for $C_v/C_s=4$. This implies that for identical envelope of performance, the range of C_v/C_s should be equal to the range of f_s/f_o squared.

III. PSPICE MODEL

To ease the study, a PSPICE model was first calibrated experimentally to follow a commercial voltage dependent CC. The CC (GRM31MR72A474KA35L) was first tested to extract its voltage dependence. The set up (Fig. 5), used to measure the CC under test (C_{UT}), is based on a voltage divider. It includes an excitation source V_{exc}, a series resistor R_{ser}, an isolating capacitor C_i, sense resistor R_s, and a relatively large resistor R_v, through which the bias voltage, V_{bias}, is fed.

In this experiment, a laboratory DC voltage supply is used for V_{bias}, whereas V_{exc} is generated by a laboratory voltage signal generator set to a sinusoidal output at a frequency of 100kHz. The amplitude of V_{exc} was rather small, so the high frequency component of the capacitor's voltage in these measurements was in the range 0.1Vrms-0.25Vrms. The voltages at points A and B, referred to ground, were measured by an oscilloscope and the obtained values were used to calculate the incremental capacitance for each bias voltage. The measured $C_d=f(V_{bias})$ data (dots in Fig. 6) was then applied to set up a PSPICE model of the variable capacitor under test (Fig. 7), implemented by inserting the points $\{(C_{d1}, V_{Bias1}), (C_{d2}, V_{Bias2}), \ldots (C_{dn}, V_{Biasn})\}$ into the Table of E7.

The simulation model of a voltage dependent capacitor was constructed by non-linear cloning of a linear capacitor as described in [30]. In this model (Fig. 7) the behavior of a voltage dependent capacitor C11 is emulated using a linear capacitance C4 which is exposed to the same voltage as C11 (C4 is fed by the voltage dependent source E6 which replicates the voltage across the C11).

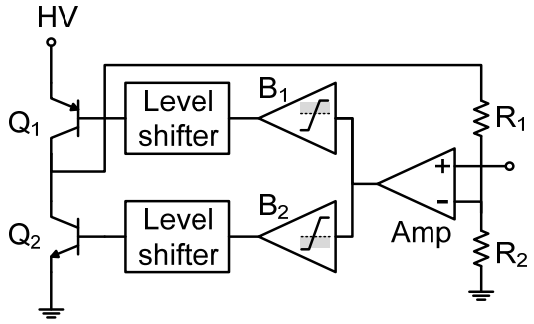

Fig. 4. Block diagram of the proposed capacitor driver.

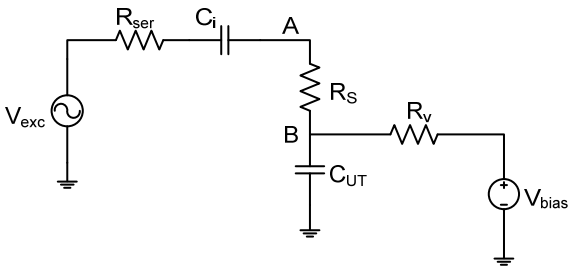

Fig. 5. Laboratory set up used to measure capacitance-to-voltage relationship of the C_{UT}.

The current of the emulated capacitor C11 is determined by a voltage-dependent current source G6. The input to G6 is the current of the reference capacitor C4 times the voltage V(Cd), set by the ETABLE voltage-dependent source E7, which replicates numerically the $C_d=f(V_{bias})$ behavior of the CC. Hence,

$$i(C11)=V(Cd)\cdot i_{C4}=V(Cd)\cdot\left(C4\frac{dV_{C4}}{dt}\right) \tag{4}$$

Since the voltages across C11 and C4 are equal:

$$i(C11)=[C4\cdot V(Cd)]\frac{dV_{C11}}{dt} \tag{5}$$

It follows from (5) that in this model the capacitance of C11 is equal to the capacitance of C4, modified by V(Cd) which represents the $C_d=f(V_{bias})$. If C4 is set to unity (i.e. 1F), the capacitance of C11 is numerically equal to V(Cd).

$$C11=C4\cdot V(Cd)=C_d \tag{6}$$

The model was first tested by reproducing the original data (dots in Fig. 6). The excellent match verifies the ability of the PSPICE model to emulate the static behavior of the C_{UT}.

A verification of the PSPICE model was carried out by comparing an experimentally recorded step response to the simulated one. Fig. 8 shows the accuracy of the PSPICE model both in the dynamic and static senses.

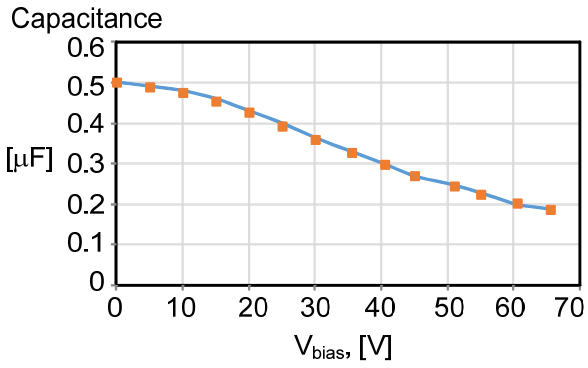

Fig. 6. Voltage dependence of the experimental CC. Dots: experiment values; Solid line: SPICE simulated.

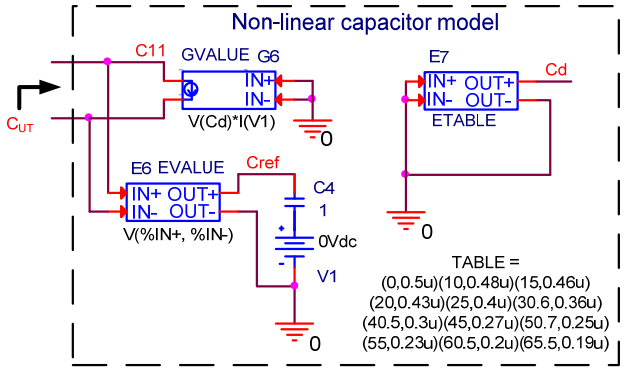

Fig. 7. PSPICE model of the C_{UT} built to follow the response of Fig. 6

The excellent matches between the experimental and simulation results validate the assessment that the PSPICE model (Fig. 7) is accurate, and it can thus emulate faithfully the behavior of the CC in a physical system. This justifies the present approach of simulation in lieu of hardware experiments.

IV. Behavior of CC Controlled SRC

As described above, the capacitance of the experimental CC, shown in Fig. 6, was measured under small AC excitation. However, the voltage change across the capacitor, while operated in resonant circuitry may be noticeably large - depending on the current of the resonant network. Consequently, since the voltage-capacitance dependence is non-linear, the curve, presented in Fig. 6 may not reflect the actual effective large signal capacitance [30, 31].

The difference between the large and small signal capacitance can be illuminated by considering charge-voltage characteristic of the experimental CC, depicted in Fig. 9.

Considering some bias voltage V_C (point C, Fig. 9), when the excitation is very small, as in Fig. 6, the effective capacitance, denoted here as small signal capacitance, C_d, will coincide with the local derivative at that point:

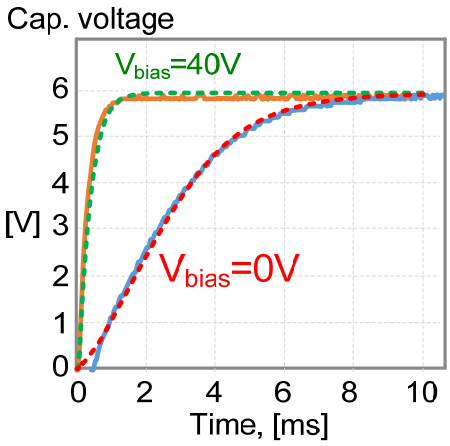

Fig. 8. Response of the CC to a step voltage drive via a resistor. Solid line: experimental; Dotted line: simulation.

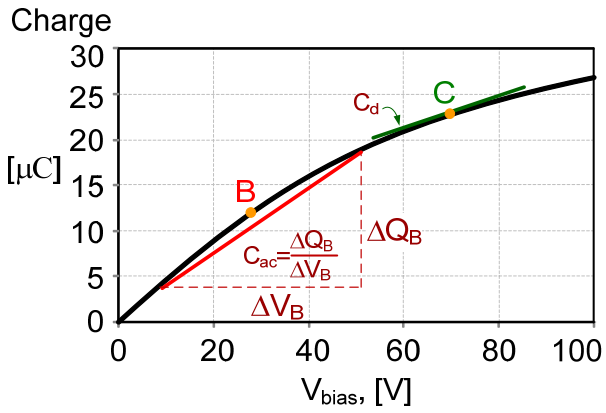

Fig. 9. Charge-voltage characteristic of experimental CC and definition of small and large signal capacitances C_d and C_{ac}.

$$C_d = \frac{dQ}{dV} \tag{7}$$

which is represented by the slope at point C in Fig. 9.

Large voltage variations of the capacitor's voltage, as those found in the resonant converter, call for different definition of the capacitance. In this case, due to the large charge's change, the capacitance cannot be represented by a local derivative. This capacitance is denoted here as a large signal capacitance C_{ac}. For a given bias voltage V_B (point B, Fig. 9), and assuming that due to the voltage changes, the charge variation is ΔQ_B, the 'effective' large signal capacitance, C_{ac}, is defined as:

$$C_{ac} = \frac{\Delta Q_B}{\Delta V_B} \tag{8}$$

The large signal capacitance C_{ac} of the experimental capacitor for different AC and bias voltages is presented in Fig. 10.

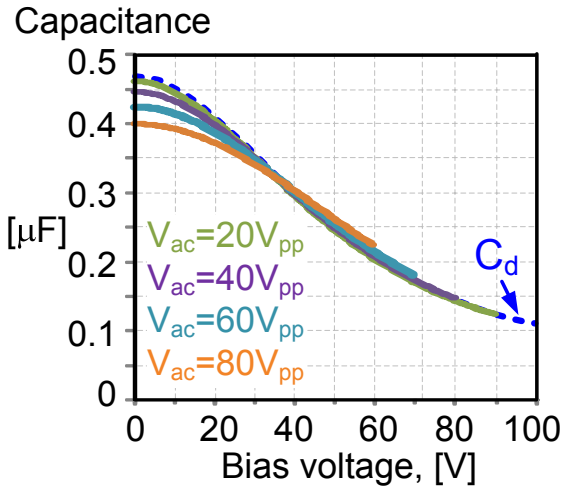

Fig. 10. Large signal capacitance C_{ac} as function of bias voltage and AC voltage of experimental CC. Dashed line: C_d; Solid lines: C_{ac} for AC voltages from $20V_{pp}$ (top line) up to $80V_{pp}$ (bottom line).

As predicted, the higher the voltage variations (AC voltage) across the capacitor, the larger the difference between the small- and the large signal capacitances. However due to the relatively small non-linearity of the charge-voltage characteristic of the experimental capacitor (Fig. 9), this difference is small, unless the AC voltage is really large. That is, even for 80V peak-to-peak AC voltage, which is 80% of the capacitor's voltage rating, the maximum difference is less than 20% (Fig. 10). This suggests that for the capacitor considered in this study, the design of the converter can be based on the small signal capacitance C_d (Fig. 6).

The control range of the experimental CC in a SRC is depicted in Fig. 11. Fig. 11a corresponds to the case when C_{r1} is fixed and $C_{r1} >> C_{r2}$, whereas in Fig. 11b both capacitors are voltage dependent. In the latter case the input voltage of 12V has been assumed. Since the input voltage is relatively small, for the bias voltages of 20V and up, the voltages across C_{r1} and C_{r2} are virtually the same.

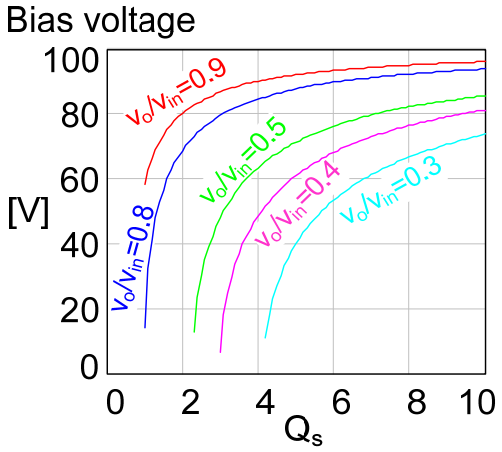

(a)

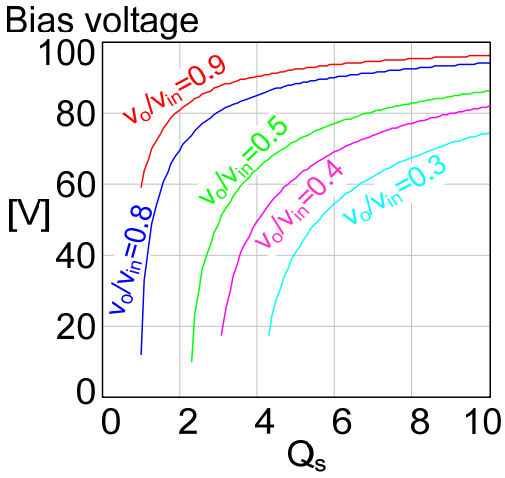

(b)

Fig. 11. Control range capability of experimental CC when applied in SRC. (a) C_{r1} is fixed, C_{r2} is voltage dependent (b) Cr1 and Cr2 are voltage dependent.

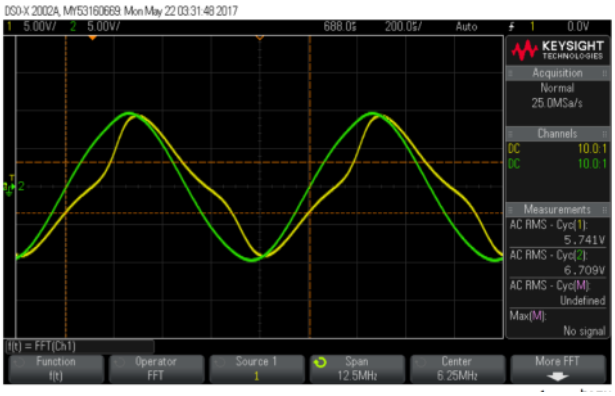

Fig. 12. Voltage of a 1μF CC driven by a sinusoidal voltage source of $10V_{pk}$ and a frequency of 1kHz, via a 220Ω resistor.

Consequently, the overall range of change of the capacitance in response to the applied bias, in two options, is very close, which explains the similarity of 11a and 11b.Higher input voltage will modify the control at low bias region in the case when both C_{r1} and C_{r2} are voltage dependent (Fig. 11b). It should be noted that since the capacitor's voltage rating cannot be exceeded, the bias voltage needs to be limited so as to allow enough space for the AC amplitude. For example, considering the capacitor explored in this study which has a rating of 100V max, the peak capacitor voltage plus the maximum bias voltage should not exceed 100V.

When the CC is driven by large signal, the nonlinearity exhibits itself as a distortion of the CC waveforms (Fig. 12). The distortion is a function of the curvature of C=f(V). When driven by a sinusoidal voltage, $v = v_a \sin(\omega t)$, the current, i, for a linear segment is (9) and for a second order segment is (10)

$$i = C_0\omega\cdot\left(v_a\cos(\omega\cdot t)+\frac{kv_a^2}{2}\sin(2\omega\cdot t)\right) \tag{9}$$

$$i = C_0\omega\cdot[v_a\cos(\omega\cdot t)+\frac{k_1v_a^2}{2}\sin(2\omega\cdot t) + \frac{k_2v_a^3}{4}(\cos(\omega\cdot t)-\cos(3\omega\cdot t))] \tag{10}$$

where k, k_1, and k_2 are the coefficients of the first order or second order curve fitting of the capacitance-voltage relationship, and C_0 is the non-biased capacitance.

Fig. 13a shows the current THD in the SRC of this study when driven by a half bridge (Fig. 1c) as a function of Q for different CC bias voltages. Fig. 13b shows the ratio between the current THD of the CC controlled SRC and the THD of a SRC with a fixed capacitor. The ratio increases with Q because the THD with fixed capacitor decreases while the nonlinearity of the CC still introduces distortion. However, the absolute THD values at large Q values for moderate voltage deviation across the CC are still small (Fig. 13a). It can thus be concluded that the non-linearity of practical CC, will have only a minor effect on the operation of the SRC.

V. Conclusion

The viability of applying a standard commercial CC for controlling resonant networks has been examined. Unlike the traditional SRC, this approach allows operation at fixed frequency while the control is done by shifting the resonant frequency of the network using a variable capacitance. It is shown that variable capacitance can be obtained by applying a bias voltage between two serially connected commercial CC, by means of DC voltage driver that has a high output impedance. The analysis of the capacitance controlled SRC, carried out in this study, indicates that the switching frequency should be set equal to the resonant frequency of the smallest expected capacitance value. This way, the converter is operated above the resonant frequency over the entire control range which, similar to the traditional SRC, assists ZVS.

The behavior of the capacitor controlled SRC was further examined by an experimentally calibrated PSPICE model of a commercial capacitor GRM31MR72A474KA35L (Murata).

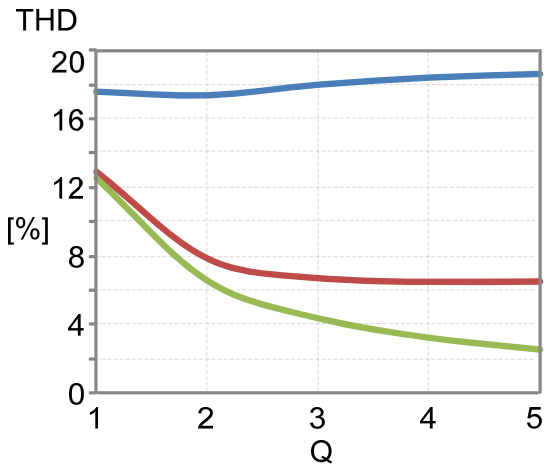

(a)

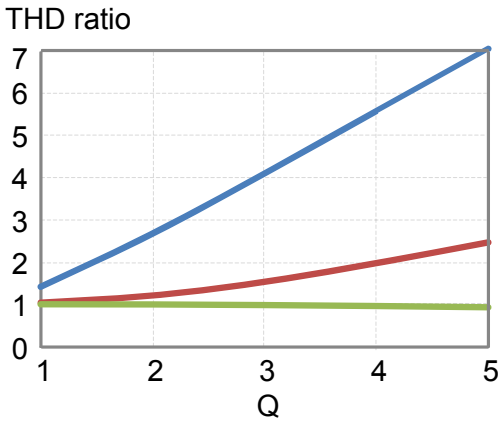

(b)

Fig. 13. Current THD as function of Q; f_s=f_o=100kHz; (a) of CC controlled SRC. V_{cap} p-p=40V; Upper trace: 40V bias; Middle trace: 20V bias; Lower trace: 0V bias. (b) THD ratio of the current of the CC controlled SRC to the current THD of a SRC with a fixed capacitor. CC operational point as in (a).

The present study demonstrates that even though the variable capacitor of the proposed SRC is exposed to relatively large AC signals, the design of the converter can be based on the small signal capacitance, provided by manufacturer's data sheets or measured by injecting a small AC excitation at different bias voltages.

The results of this study show that control attributes of the capacitor controlled SRC are identical to those of the conventional, frequency controlled, SRC, when taking into account that $\frac{f_s}{f_o} = \sqrt{\frac{C_v}{C_s}}$. Based on the present investigation, C_v/C_s ratios of 1:5 can be practically achieved. This implies that the performance of the capacitor controlled SRC would be comparable to the conventional SRC in which the range of f_s/f_o is about 1:2.2 It is further found that the non-linearity of practical CC, has only a minor effect on the operation of the SRC.

REFERENCES

[1] D. Medini and S. Ben-Yaakov, "A current-controlled variable-inductor for high frequency resonant power circuits," in *IEEE Applied Power Electronics Conference*, 1994, pp. 219-225.

[2] M. Martins, M. S. Perdigao, A. M. S. Mendes, R. A. Pinto, J. M. Alonso, "Analysis, design, and experimentation of a dimmable resonant-switched-capacitor LED driver with variable inductor control," *IEEE Transactions on Power Electronics*, vol. 32, no. 4, 2017.

[3] J. M. Alonso, M. S. Perdigao, G. Z. Abdelmessih, M. A. D. Costa, Y. Wang, "SPICE modeling of variable inductors and its application to single inductor LED driver design," *IEEE Transactions on Industrial Electronics*, vol. 64, no. 7, 2017.

[4] K. Harada, A. Katsuki, M. Fujiwara, H. Nakajima and H. Matsushita, "Resonant converter controlled by variable capacitance devices," in *21 Annual IEEE Conference on Power Electronics Specialists*, 1990, pp. 273-280.

[5] A. Katsuki, K. Shirouzu, K. Harada and M.Fujiwara, "Improved variable capacitance device and its applications to resonant converters," in *Intelec 93: 15th International Telecommunications Energy Conference*, 1993, vol. 2, pp. 242-246.

[6] K. Harada; A. Katsuki; M. Fujiwara; H. Nakajima; H. Matsushita "Resonant converter controlled by variable capacitance devices," *IEEE Transactions on Power Electronics*, vol, 8, no. 4, pp. 404–410, 1993.

[7] A. Katsuki and T. Oki, "Leakage current suppression in the variable capacitance device for the use in AC power converters," in *IEEE 10th International Conference on Power Electronics and Drive Systems (PEDS)*, 2013, pp. 90-95.

[8] A. Katsuki and T. Oki, "Suppression of Leakage Current and Distortion in Variable Capacitance Devices and their Application to AC Power Regulators," Journal of power Electronics, vol. 16, no. 1, pp. 66-73, 2016.

[9] W. Xusheng, Z. Ming, R. Xiaojiao, F. Rodes, R. Denieport, "Auto tuning system for a half bridge resonant converter using a synchronous switched capacitor," in *IEEE 13th International New Circuits and Systems Conference*, 2015, pp. 1-4.

[10] Y. Hu, A. Amara, A. Ioinovici, "LLC resonant converter operated at constant switching frequency and controlled by means of a switched-capacitor circuit," in *1st International Future Energy Electronics Conference (IFEEC)*, 2013, pp. 691–696.

[11] M. Fortunato, "Temperature and voltage variation of ceramic capacitors, or why your 4.7µF capacitor becomes a 0.33µF capacitor," [Online]. Available: http://pdfserv.maximintegrated.com/en/an/TUT5527.pdf

[12] S. Kwon, W. Hackenber, E. Alberta, E. Furman, M. Lanagan, "Nonlinear dielectric ceramics and their applications to capacitors and tunable dielectrics," *IEEE Electrical Insulation Magazine*, vol. 47, pp. 43-45, 2011.

[13] O. Dejean, T. Lebey, "An experimental characterization of nonlinear ceramic capacitors for small and large signals," *IEEE Transactions on Components and Packaging Technologies*, vol. 23, no. 4, 2000.

[14] L. Dai, F. Lin, Z. Zhu, and J. Li, "Electrical characteristics of high energy density multilayer ceramic capacitor for pulse power applications," *IEEE Transactions on Magnetics*, vol. 41, no. 1, 2005.

[15] P. W. Tuinenga, SPICE: A Guide to Circuit Simulation and Analysis Using PSPICE. New Jersey: Prentice Hall, 1988.

[16] C. K. Campbell, J. D. van Wyk, M. F. K. Holm and J. J. Schoeman, "Aspects of modeling of high voltage ferroelectric nonlinear ceramic capacitors," *IEEE Transactions on Components, Hybrids, and Manufacturing Technology*, vol. 15, pp. 245-251, 1992.

[17] U. Drofenik, A. Müsing and J. W. Kolar, "Voltage-dependent capacitors in power electronic multi-domain simulations," in *The 2010 International Power Electronics Conference*, 2010, pp. 643-650.

[18] D. Biolek, Z. Kolka, V. Biolkova, "Modeling time-varying storage components in PSpice," [Online]. Available: https://user.unob.cz/biolek/veda/articles/eds07.pdf.

[19] D. Costinett, D. Maksimovic and Regan Zane, "Circuit-Oriented Treatment of Nonlinear Capacitances in Switched-ModePower Supplies," *IEEE Transactions on Power Electronics*, vol. 30, pp. 985-995, 2015.

[20] H. Mann, "Circuit model of energy-storing transducers," in *1995 IEEE International Symposium on Circuits and Systems (ISCAS)*, 1995, vol. 2, pp. 1271-1274.

[21] Y. Kulvitit, "Energy capapacity of voltage dependent capacitor for the calculation of MOSFET's switching losses," in *IEEE International Conference on Electron Devices and Solid State Circuit (EDSSC)*, 2012, vol. 30, pp. 1-4.

[22] M. A. Stošović, M. Dimitrijević and V. Litovski, "SPICE Model of a Linear Variable Capacitance," in *The 5th Small Systems Simulation Symposium*, pp. 43-46, 2014.

[23] Variable Capacitor. MathWorks, MA, USA. "Variable Capacitor – Model linear time-varying capacitor," [Online]. Available: https://www.mathworks.com/help/physmod/elec/ref/variablecapacitor.html

[24] Cadence, "Modeling Voltage-Controlled Resistors and Capacitors in PSpice," [Online]. Available: http://www.pspice.com/resources/application-notes/modeling-voltage-controlled-resistors-and-capacitors-pspice.

[25] S. Pearson, A. Laprade, "Tips and Tricks to Get More Out of Your SPICE Models," Fairchild Power Seminar, 2007.

[26] C. Basso. (2005, May). SPICE Analog Behavioral Modeling of Variable Passives. Power Electronics Technology [Online]. Available: http://www.powerelectronics.com/content/spice-analog-behavioral-modeling-variable-passives.

[27] L. Zhang, A. Ritter, C. Nies, S. Dwari, B. Guo, S. Priya, R. Burgos and K. Ngo, "Voltage-controlled capacitor—feasibility demonstration in DC–DC converters," *IEEE Transactions on Power Electronics*, vol. 32, no. 8, pp. 5889–5892, 2017.

[28] U. Drofenik, A. Müsing and J. W. Kolar, "Voltage-dependent capacitors in power electronic multi-domain simulations," in *The 2010 International Power Electronics Conference*, 2010, pp. 643-650.

[29] R. L. Steigerwald, "A comparison of half-bridge resonant converter topologies," in *The 2nd IEEE Applied Power Electronics Conference and Exposition*, 1987, pp. 135-144.

[30] Zeltser, I., Ben-Yaakov, S., "On SPICE simulation of voltage dependent capacitors," in *IEEE Transactions on Power Electronics*. To be Published. [Online]. Available: http://www.ieeexplore.ieee.org/stamp/stamp.jsp?tp=&arnumber=8081815

[31] Ben-Yaakov, S., "'Capacitance' definition of voltage dependent capacitors: The fundamental Q=f(V) curve," [Online]. Available: https://youtu.be/bAYbHmuWlps